Supporting Information

On-demand optical generation of single flux quanta

Antonine Rochet[1,2], Vasiliy Vadimov[3], William Magrini[1,2], Siddharatha Thakur[1,2], Jean-Baptiste Trebbia[1,2], Alexander Melnikov[3,4], Alexander Buzdin[5], Philippe Tamarat[1,2] and Brahim Lounis[1,2]

[1] *Université de Bordeaux, LP2N, F-33405 Talence, France*
[2] *Institut d'Optique & CNRS, LP2N, F-33405 Talence, France*
[3] *Institute for Physics of Microstructures, Russian Academy of Sciences, 603095 Nizhny Novgorod, GSP-105, Russia*
[4] *Sirius University of Science and Technology, 1 Olympic Ave, 354340 Sochi, Russia*
[5] *University of Bordeaux, LOMA UMR-CNRS 5798, F-33405 Talence, France*

Methods

Magneto-optical imaging of Abrikosov vortices

The magneto-optical contrast depends on the extinction ratio of the ensemble polarizer-lens-crossed analyzer[1,2]. The extinction ratio is typically ~10^{-3}.[3] To enhance the contrast of magneto-optical imaging, a background subtraction procedure is used to suppress the contribution of defects at the sample surface and non-uniformity of the sample illumination. An image taken at $T>T_c$ is subtracted from all raw images recorded at $T<T_c$ under the same conditions. To improve the signal-to-noise ratio, an average is performed over 50 images with an integration time of 10 ms. The magneto-optical signal is coded with a color scale bar, without any filtering process.

Numerical simulations of the KZ nucleation and separation of a vortex-antivortex pair

In order to model the nucleation of vortex-antivortex pairs and their separation in the presence of Meissner currents, we have performed numerical simulations of the temporal evolution of the order parameter Ψ in the superconducting film, which is governed by the time-dependent Ginzburg-Landau equations [4,5]

$$\begin{cases} \tau_\Psi\left(\frac{\partial}{\partial t} - i\frac{2\pi}{\Phi_0}\varphi\right)\Psi = \frac{-T_c - T(\boldsymbol{r},t)}{T_c - T_0}\Psi + |\Psi|^2\Psi + \xi^2\left(-i\nabla - \frac{2\pi}{\Phi_0}\mathbf{A}\right)^2\Psi + f(\boldsymbol{r},t) \\ \sigma_n\nabla^2\varphi + \frac{1}{\mu_0\lambda_L^2}\mathrm{div}\left[\frac{\Phi_0}{2\pi}i\left(\Psi^*\nabla\Psi - \Psi\nabla\Psi^*\right) + \mathbf{A}|\Psi|^2\right] = 0 \end{cases},$$

where φ is the electric potential, $\mathbf{A}$ the vector potential, τ_Ψ the zero-temperature relaxation time of the order parameter, ξ the coherence length, λ_L the London penetration depth, Φ_0 the flux quantum and σ_n the normal electric conductivity of the film. The function f introduces a source of noise to simulate the thermal fluctuations present in the regime of instability inherent to the Kibble-Zurek scenario. It is such that $\langle f(\boldsymbol{r},t)f(\boldsymbol{r}',t')\rangle = \left(16\mu_0 k_B T_c\tau_\Psi\xi^2\lambda_L^2/\Phi_0^2\right)\delta(\boldsymbol{r}-\boldsymbol{r}')\delta(t-t')$. The pinning potentials in the superconductor are taken into account by introducing a static coordinate-dependent random noise in the critical temperature $T_c(\boldsymbol{r})$. In order to have a qualitative description of the non-equilibrium dynamics of the superconductor, we make the following assumptions:

i) In the heat equation, we neglect the feedback term associated to the temporal evolution of the vector potential [6], and take into account lateral heat diffusion in the superconductor and heat evacuation into the substrate on which the superconductor is grown. The solution is a spatial and temporal Gaussian 2D-profile of temperature subsequent to the absorption of a laser pulse:

$$T(r,t) = T_0 + \frac{(T_{\mathrm{peak}} - T_0)r_0^2}{r_0^2 + Dt} exp\left(\frac{-r^2}{r_0^2 + Dt} - \gamma t\right)$$

where T_{peak} is the initial temperature at the hotspot center, T_0 the base temperature of the sample, r_0 the radius of the hotspot, D the thermal diffusivity of the superconductor film and γ the rate of heat drain. Due to the efficient heat evacuation into the sapphire substrate, we can neglect the thermal diffusivity of the Nb film.

ii) We neglect the contribution of Meissner currents to the vector potential by assuming that the thickness of the sample is smaller than the effective penetration depth $\sim\lambda_{\mathrm{L}}^2/d_{\mathrm{S}}$.

The studied area of the superconductor is a square. One of its sides (the lowest horizontal side in the images of Fig. 4, Fig. S5 and Fig. S6) is the superconductor edge, along which Meissner supercurrents develop. The system of time dependent Ginzburg-Landau and continuity equations is discretized on a square grid with area $N \times N\ \xi^2$, where N is restricted to 200. For a given order parameter Ψ at time t, we solve the continuity equation with a Fourier method and find the electric potential φ. Then, using φ we find the order parameter at time $t + dt$ with the semi-implicit Crank-Nicolson method. First we find the equilibrium distribution of the order parameter in the external magnetic field, and then we start the simulation of the superconductor dynamics heated by the laser pulse.

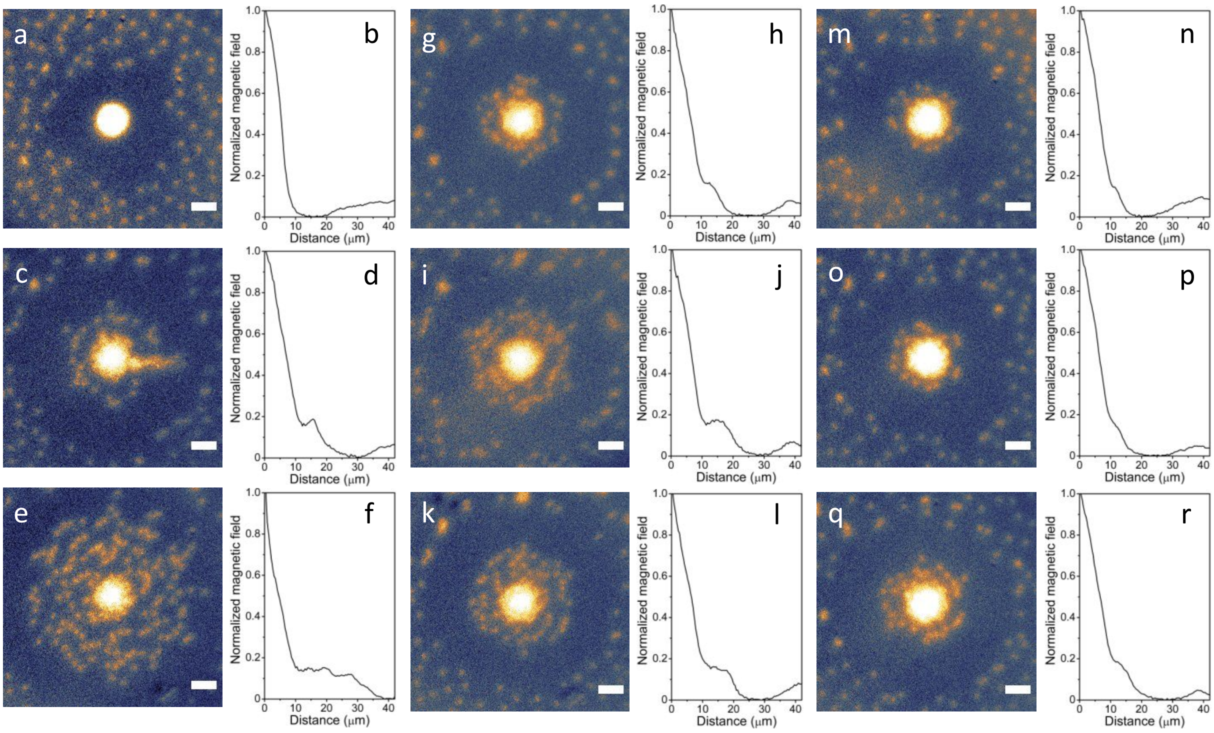

Figure S1. Magnetic flux shaping with a focused laser pulse.
Starting from a random vortex distribution obtained after field cooling of Nb film below T_c, the magneto-optical images are recorded after the application of a laser pulse (wavelength 532 nm, duration 200 ps) tightly focused at the center of the images. Their averaged radial distributions of magnetic field are displayed. For this series, the applied field is 0.4 Oe. (a, c, e) are the same as those displayed in Fig. 1 (c, d, e), respectively. The pulse energy is 0.8 nJ (a,b), 2.9 nJ (c,d), 6.6 nJ (e,f), 2.2 nJ (g,h), 3 nJ (i,j,k,l), 1.8 nJ (m,n,o,p), 2.2 nJ (q,r). The images and field profiles show evidence for magnetic flux redistribution in the form of multiple-ring vortex patterns formed in the cooling process. They map the instabilities of the order parameter phase that develop during the quench in the region between the temperature front and the order parameter front, which converge to the hotspot center with different speeds.[6,7] All scale bars are 10 μm.

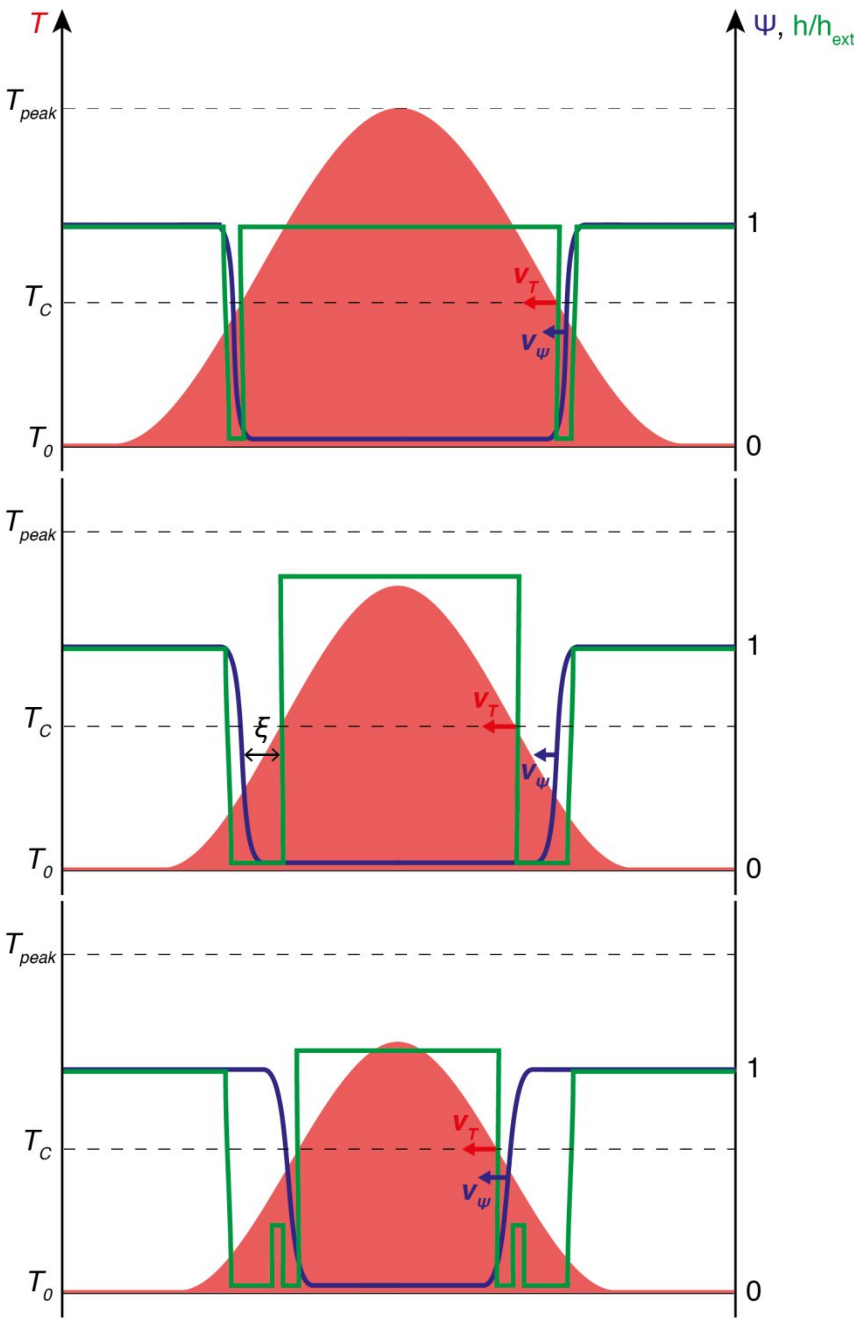

Figure S2. Schematic of temporal evolution of the magnetic field penetration through the superconducting region after the laser pulse.

While the temperature profile (red curve) collapses, the profile of the order parameter (blue curve) tightens. The critical temperature front (where the temperature equals T_{c}) converges to the hotspot center faster than the order parameter front, due to the slow response time of superconductivity when the temperature is close to T_{c}. The magnetic field h (normalized to the external field) trapped in the normal region increases (green levels) and contributes to slow down the order parameter front. Fluctuations of the order parameter phase develop in the region between these two fronts. When the separation between fronts exceeds the superconducting coherence length ξ, these fluctuations generate vortices that get trapped in a ring-shaped pattern. Such a flux release reduces the topological charge of the normal domain and accelerates the order parameter front, which sweeps the phase fluctuations and the nucleating vortices, and presses the remaining magnetic flux in the hotspot until it slows down again. New vortex rings may be generated upon the repetition of this scenario during the process of superconductivity recovery.

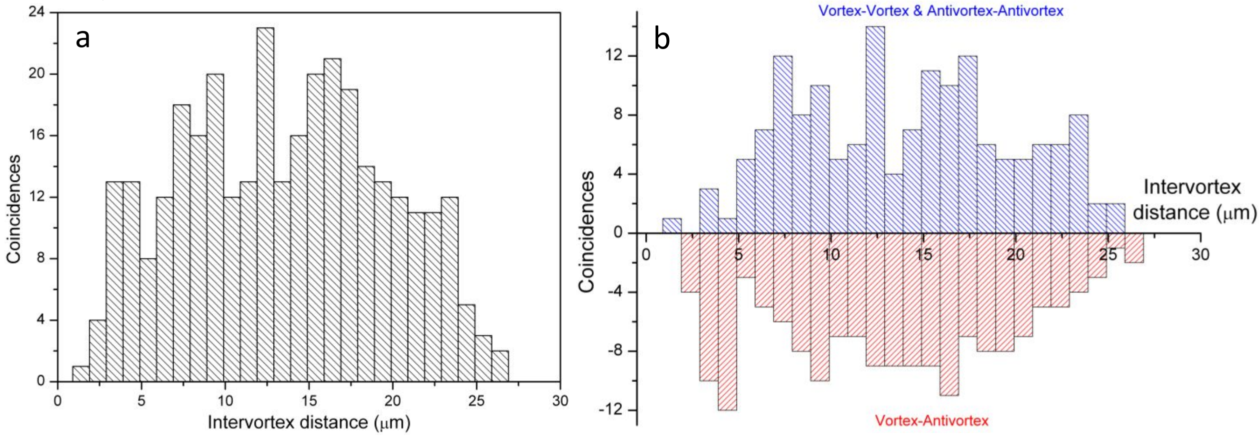

Figure S3. Histograms of the intervortex distances in Figure 2b.

a, Using a bin of 1 μm, we plot for each intervortex distance the number of flux quantum pairs, regardless of their helicity. **b**, We plot for each intervortex distance the number of flux quantum pairs multiplied by the product of their helicities. The correlation between vortices and antivortices clearly shows up at ~4μm.

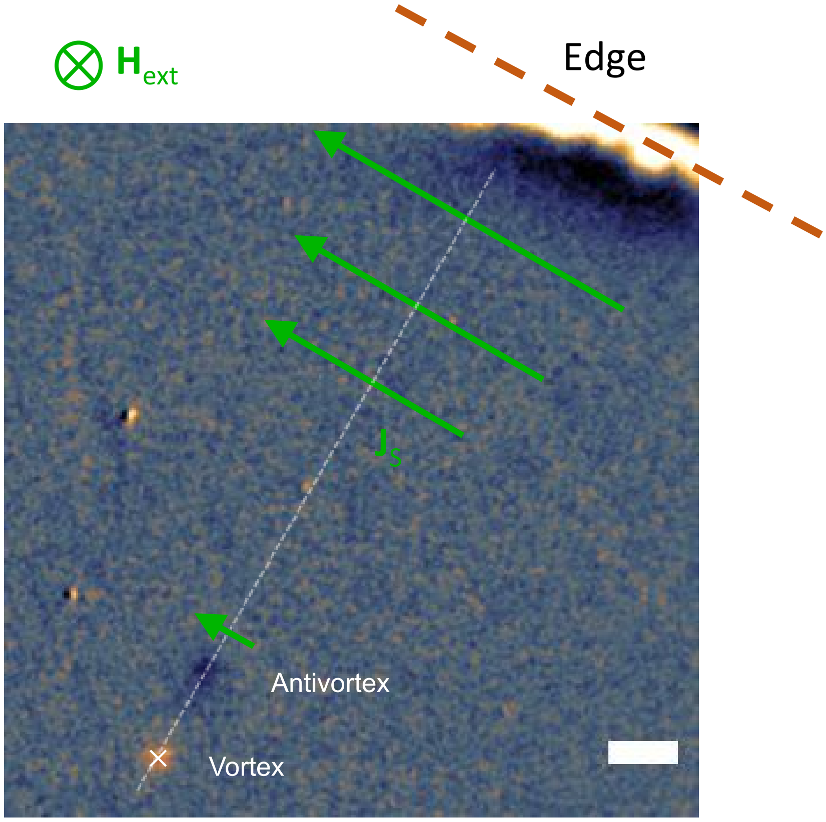

Figure S4. Controlling the orientation of a single vortex pair.
Creation of a single vortex-antivortex pair with a laser pulse (wavelength 780 nm, duration 2 ps) under a magnetic field of 0.4 Oe. The center of the hotspot is marked with a cross and located at ~100 µm from the edge of the Nb film. The pair orientation follows a direction nearly orthogonal to the sample edge. This is a signature of vortex extraction from the shrinking hotspot during the quench process, under the effect of Meissner supercurrents flowing around the normal region. The distribution and orientation of the Meissner current density $\mathbf{J}_S$ circulating close to the edge of the Nb film are illustrated with green arrows. The scale bar is 10 µm.

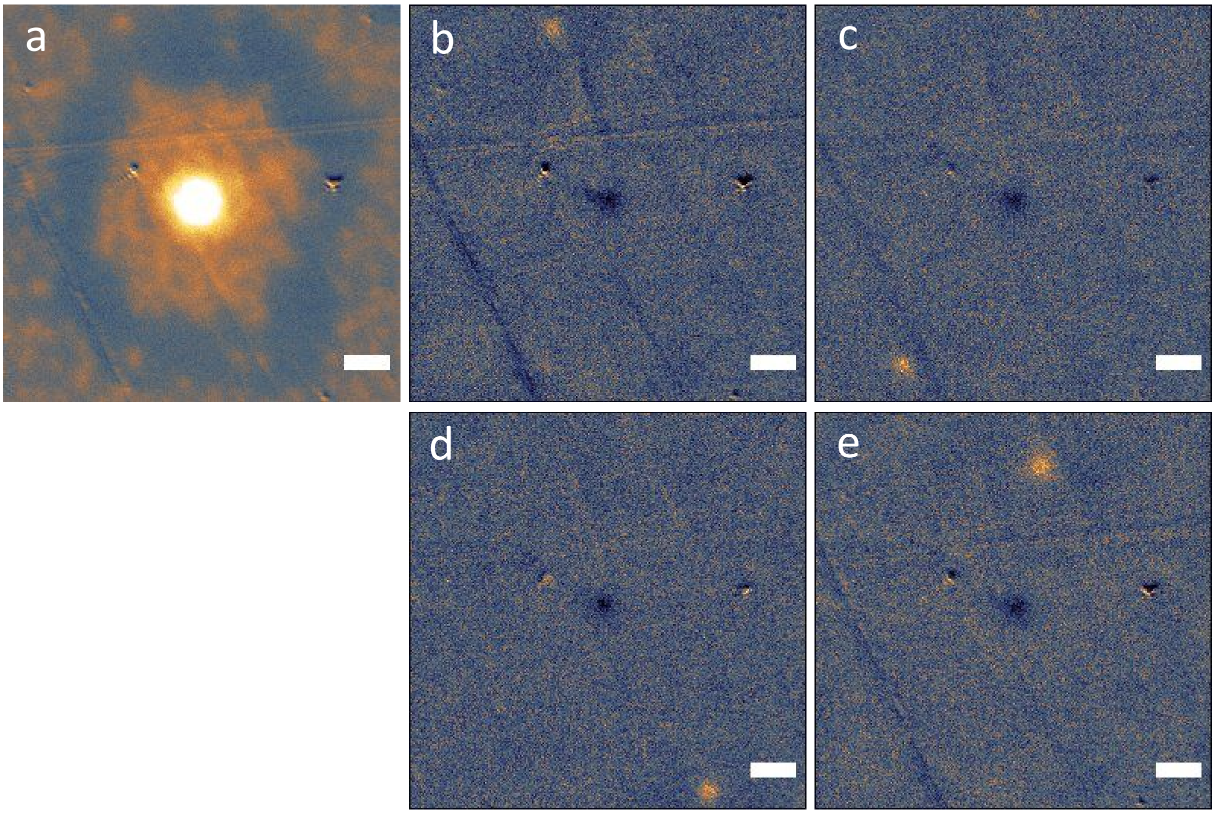

Figure S5. Generation of single flux quanta without magnetic field.
(a) Starting from a spontaneous vortex distribution formed under field cooling of the Nb film under a field of 0.7 Oe, we obtain a reshaped magnetic flux landscape after illumination with a tightly focused laser pulse (wavelength 780, duration 2 ps) with absorbed energy $E_{\mathrm{abs}} = 2.6$ nJ centered on the cross, under the same field. (b-e), Starting from a vortex-free area, examples of ex-nihilo generation of single vortices with the same pulse energy, in the absence of magnetic field. We obtain a vortex at the center of the illumination spot and a vortex with opposite flux at a random position on the boundary of the heated area. All scale bars are 10 µm.

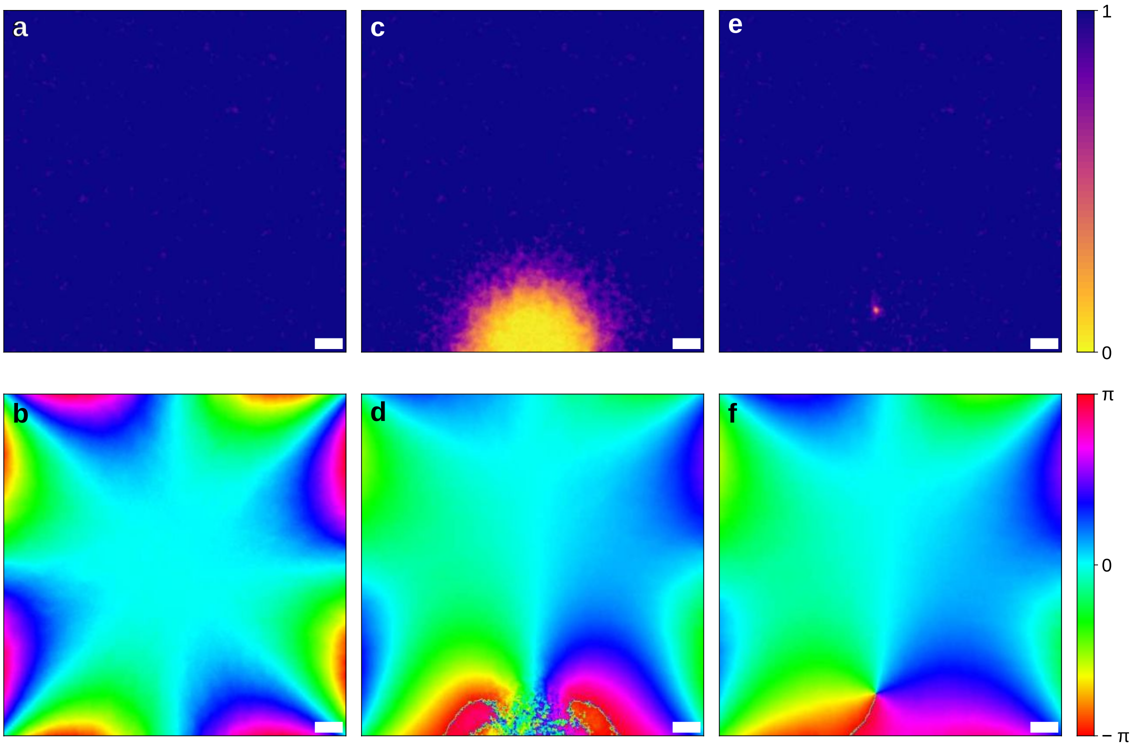

Figure S6. Creation of a vortex close to the superconductor edge.
Computed distribution of the modulus (a, c, e) and the associated phase (b, d, f, respectively) of the order parameter in the superconductor at different stages: before (a, b), during (c, d) and after (e, f) application of a laser pulse at the sample edge under an external magnetic field of 2 10^{-3} times the upper critical field. In this configuration, there is no topological protection and a vortex enters the superconductor through the boundary. No antivortex is formed in the superconductor. The simulations are performed with $(T_{\mathrm{peak}} - T_0)/(T_c - T_0) = 1.5$, $r_0 = 30\ \xi$, $\gamma = 1/(15\ \tau_\Psi)$. All scale bars are 10 ξ.

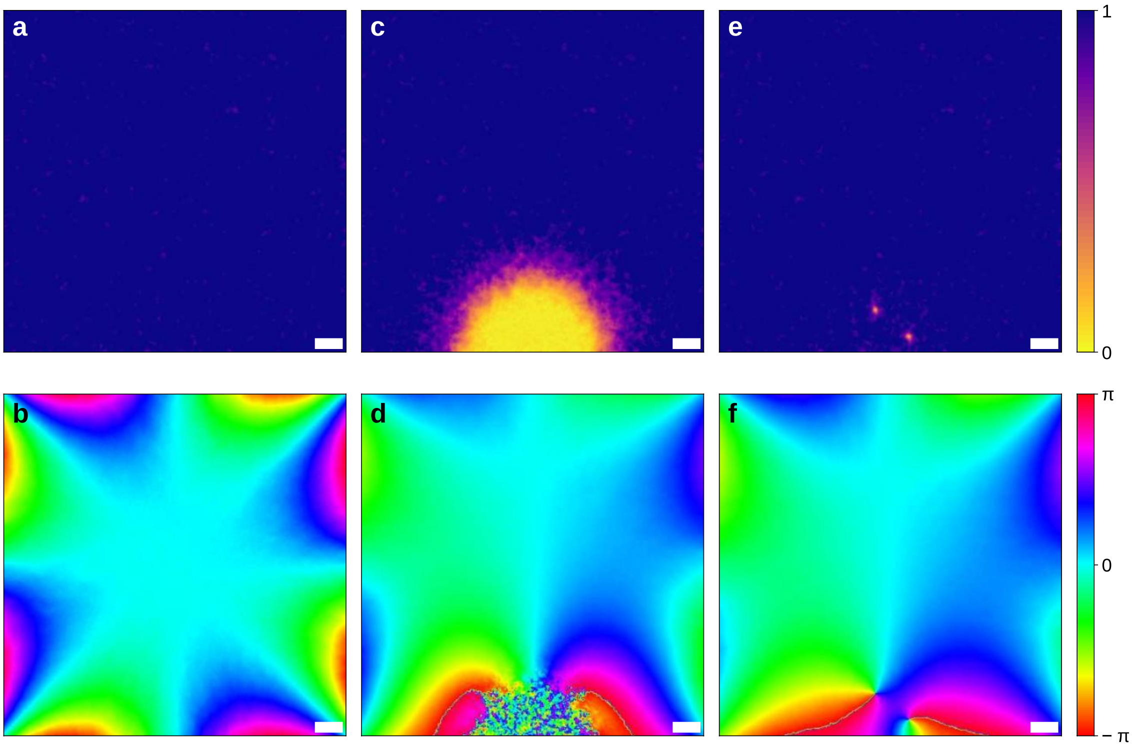

Figure S7. Creation of two vortices close to the superconductor edge.
Computed distribution of the modulus (a, c, e) and the associated phase (b, d, f, respectively) of the order parameter in the superconductor at different stages: before (a, b), during (c, d) and after (e, f) application of a laser pulse at the sample edge under an external magnetic field of 2 10^{-3} times the upper critical field. In this configuration, there is no topological protection and two vortices enter the superconductor through the boundary. No antivortex is formed in the superconductor. The simulations are performed with $(T_{\mathrm{peak}} - T_0)/(T_{\mathrm{c}} - T_0) = 2$, $r_0 = 30\ \xi$, $\gamma = 1/(15\ \tau_\Psi)$. All scale bars are 10 ξ.

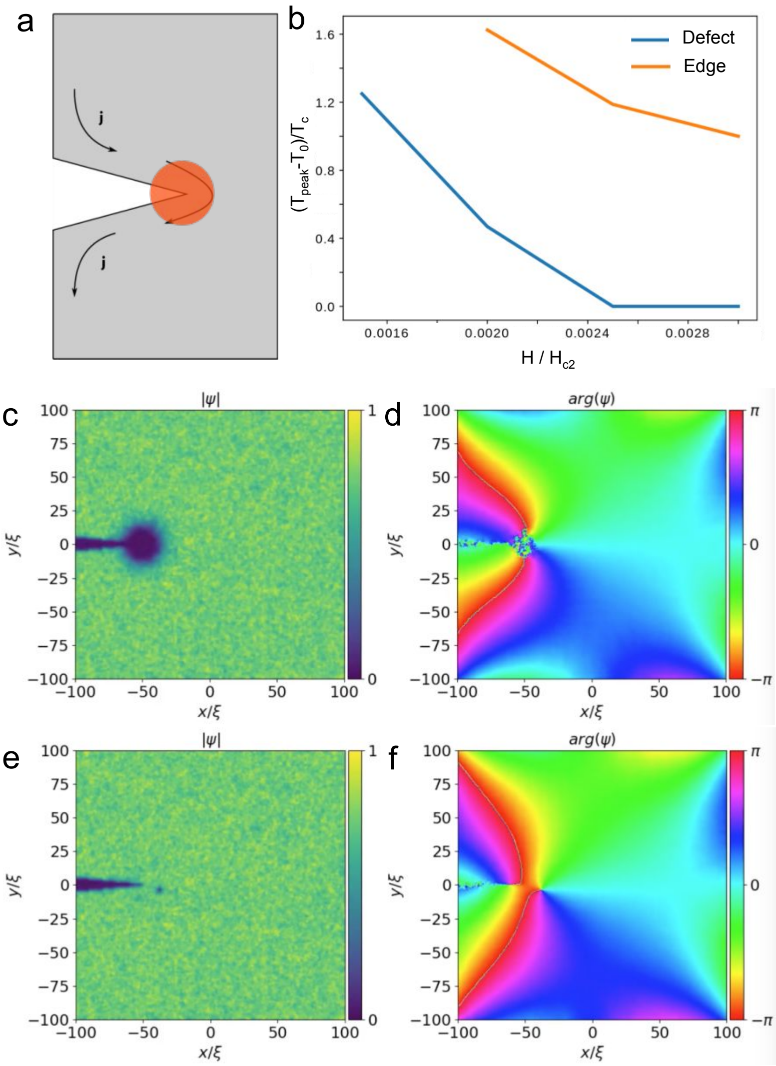

Figure S8. Triggering the creation of a single vortex near a defect.
(a) In the presence of a sharp cut-like defect at the edge of the superconductor, the screening Meissner supercurrent flows around the defect with an increased current density (black arrows). This allows triggering the entry of a single vortex with a weak increase of local temperature induced by absorption of a laser pulse focused at the defect (orange spot). (b) Using numerical simulations, we derive the minimal peak temperature within the hotspot (which is proportional to the energy absorbed by the superconductor) needed to create a vortex at the defect (blue curve) or at a plain edge (orange curve). (c) and (d) show the spatial distribution of the modulus (c) and phase (d) of the order parameter at the stage of local heating. (e) and (f) After the quench, a single vortex is formed close to the defect. These simulations are performed with an applied magnetic field of 2 10^{-2} times the upper critical field, $(T_{\text{peak}} - T_0)/(T_{\text{c}} - T_0) = 2$, $r_0 = 10\ \xi$, $\gamma = 1/(15\ \tau_\Psi)$. These images are extracted from Movie 2, which exhibits the whole nucleation process.

References

(1) Goa, P. E.; Hauglin, H.; Olsen, A. A. F.; Baziljevich, M.; Johansen, T. H. Magneto-Optical Imaging Setup for Single Vortex Observation. *Rev. Sci. Instrum.* **2003**, *74*, 141–146.
(2) Tsuchiya, Y.; Nakajima, Y.; Tamegai, T. Development of Surface Magneto-Optical Imaging Method. *Physica C: Superconductivity and its applications* **2010**, *470*, 1123–1125.
(3) Veshchunov, I. S.; Magrini, W.; Mironov, S. V.; Godin, A. G.; Trebbia, J. B.; Buzdin, A. I.; Tamarat, P.; Lounis, B. Optical Manipulation of Single Flux Quanta. *Nature Communications* **2016**, *7*, 12801.
(4) Ghinovker, M.; Shapiro, I.; Shapiro, B. Y. Explosive Nucleation of Superconductivity in a Magnetic Field. *Phys. Rev. B* **1999**, *59*, 9514–9521.
(5) Tinkham, M. Introduction to Superconductivity. *Mc-Graw Hill, New York* **1996**.
(6) Shapiro, I.; Pechenik, E.; Shapiro, B. Y. Recovery of Superconductivity in a Quenched Mesoscopic Domain. *Phys. Rev. B* **2001**, *63*, 184520.
(7) Shapiro, B.; Bel, G.; Rosenstein, B.; Shapiro, I. Hot Spot in Type-II Superconductors: Dynamics and Instabilities. *Physica C: Superconductivity* **2004**, *404*, 335–339.